CO_2 SELECTIVE CERAMIC MEMBRANE FOR WATER-GAS-SHIFT REACTION WITH CONCOMITANT RECOVERY OF CO_2

Quarterly Report
For the period October1, 2004 to December 31, 2004

Paul K. T. Liu
Project Director

January 31, 2005

PREPARED FOR THE UNITED STATES
DEPARTMENT OF ENERGY
Under Cooperative Agreement
No. DE-FC26-00NT40922

By
MEDIA AND PROCESS TECHNOLOGY, INC.
1155 William Pitt Way
Pittsburgh, PA 15238

Disclaimer

ABSTRACT

Our CO_2-affinity material synthesis activities thus far have offered two base materials suitable for hydrogen production via low temperature water gas shift reaction (LTS-WGS) with concomitant removal of CO_2 for sequestration. They include (i) a nanoporous CO_2-affinity membrane and (ii) a hydrotalcite based CO-affinity adsorbent. These two materials offer a commercially viable opportunity for implementing an innovative process concept termed the hybrid adsorbent-membrane reactor (HAMR) for LTS-WGS, proposed by us in a previous quarterly report. A complete mathematical model has been developed in this quarter to describe the HAMR system, which offers process flexibility to incorporate both catalysts and adsorbents in the reactor as well as permeate sides. In comparison with the preliminary mathematical model we reported previously, this improved model incorporates "time" as an independent variable to realistically simulate the unsteady state nature of the adsorptive portion of the process. In the next quarterly report, we will complete the simulation to demonstrate the potential benefit of the proposed process based upon the performance parameters experimentally obtained from the CO_2-affinity adsorbent and membrane de veloped from this project.

TABLE OF CONTENTS

List of Graphical Materials

Tables

Figures

1. INTRODUCTION

A preliminary mathematical model was developed and summarized in one of our previous quarterly reports, 4th quarter 2003, for the use of the CO_2-affinity membrane as a separator and reactor. In this report, we summarize our continuous effort in this area, specifically for its application in water gas shift (WGS) reaction. Our membrane synthesis activities thus far have offered two types of membranes suitably as membrane reactors for improving the efficiency of WGS for hydrogen production with the concomitant CO_2 removal for sequestration. The permeation properties of these membranes are listed as follows:

- Hydrotalcite based inorganic membranes with CO_2 affinity. Our progress thus far has indicated that defects of the membranes remain, which degrade selectivity significantly. Although the selectivity obtained thus far has been significant, i.e., beyond the Knudsen selectivity of ~0.79 for CO_2/N_2,, we believed that this level of selectivity is not economically attractive for the proposed application. Synthesis activity is on-going to minimize defects and then upgrade its selectivity.
- Inorganic membranes with CO_2 affinity. CO_2 permeance in the range of 0.3 to 1.5 $m^3/m^2/hr/bar$ has been prepared for the temperature up to 300ºC. However, due to its porous structure, the membrane also shows significant hydrogen permeance, in the range of 1 to ca.4 $m^3/m^2/hr/bar$ at the same temperature range. This membrane is presently ready for further development in scale-up and process optimization.

For the purpose of identifying commercialization opportunities for the next phase study, we will focus on the use of hydrotalcite as a CO_2-adsorbent in conjunction with the nanoporous CO_2 affinity membrane to develop a dual-enhanced process, i.e., both adsorption and membrane, to improve the hydrogen production efficiency while deliver a concentrate CO_2 stream for sequestration. Through simulation we will demonstrate that this dual enhanced process concept takes the full advantage of the CO_2 adsorbent and membrane we have developed thus far to meet the original project objectives.

2. EXECUTIVE SUMMARY

While our synthesis is on-going with the focus on the defect minimization, we have resumed our simulation activity to identify the commercialization opportunities with materials developed this far. Our CO_2-affinity material synthesis activities thus far have offered two base

materials suitable for hydrogen production via low temperature water gas shift reaction (LTS-WGS) with concomitant removal of CO_2 for sequestration. They include (i) a CO_2-affinity membrane and (ii) a hydrotalcite based CO-affinity adsorbent. These two materials offer a commercially viable opportunity for implementing an innovative process concept termed the hybrid adsorbent-membrane reactor (HAMR) for LTS-WGS, proposed by us in a previous quarterly report. A complete mathematical model has been developed to describe the HAMR system, which offers process flexibility to incorporate both catalysts and adsorbents in the reactor as well as permeate sides. In comparison with the preliminary mathematical model we reported previously, this improved model incorporates "time" as an independent variable to realistically simulate the unsteady state nature of the adsorptive portion of the process. In the next quarterly report, we will complete the simulation to demonstrate the potential benefit of the proposed process based upon the performance parameters experimentally obtained from the CO_2-affinity adsorbent and membrane developed from this project. Our simulation will focus on the yield and purity of (i) the hydrogen stream as a product and (ii) the CO_2 stream for sequestration.

3. EXPERIMENTAL: LITERATURE REVIEW ON HYBRID REACTOR

Reactive separation processes have been attracting renewed interest for application in catalytic steam reforming primarily. They include packed-bed catalytic membrane reactors[10-15], and more recently adsorptive reactor (AR) processes[16-26]. Their potential advantages, over the more conventional reformers have been widely discussed. They include, (i) increasing reactant conversion and product yield, through shifting the equilibrium towards the products, potentially allowing one to operate under milder operating conditions (e.g., lower temperatures and pressures, and reduced steam consumption), and (ii) reducing the downstream purification requirements by *in-situ* separating from the reaction mixture the desired product hydrogen (in the case of membrane reactors), or the undesired product CO_2 (in the case of adsorptive reactors).

Membrane reactors (MR) show substantial promise in this area and, typically, utilize nanoporous inorganic or metallic Pd or Pd-alloy membranes[15]. The latter are better suited for pure hydrogen production. However, metallic membranes are very expensive, and become brittle during reactor operation[13], or deactivate in the presence of sulfur or coke. Nanoporous membranes are better-suited for the steam-reforming environment. They are difficult to manufacture, however, without cracks and pinholes, and as a result often have inferior product yield. In addition, the hydrogen product in the permeate side contains substantial amounts of other by-products, particularly CO, and may require further treatment for use in fuel-cell-powered vehicles.

Adsorptive methane steam reforming reactors also show good potential[16-20]. The challenge here, however, is in matching the adsorbent properties with those of the catalytic system. Two types of adsorbents have been suggested: potassium-promoted layered-double hydroxides (LDH), which operate stably only at lower temperatures (less than 500 °C [25-27]), and CaO or commercial dolomite, which can be utilized at the typical steam reforming temperatures of 650 – 700 °C[21], but requires temperatures higher than 850 °C for regeneration[23-24]. These are very harsh conditions that result in gradual deterioration of the adsorbent properties, and potentially sintering of the reforming catalyst[9,23-24]. The mismatch between the reaction and regeneration conditions is likely to result in significant process complications.

Based upon the above literature review, what we propose for use is a novel reactor system, termed the hybrid adsorbent-membrane reactor (HAMR). Our HAMR system involves a hybrid packed-bed catalytic membrane reactor, coupling the water-gas-shift reaction through a gas separation membrane with a CO_2 adsorption system. Our porous CO_2-affinity membrane and

the hydrotalcite based CO_2-adsorbent will be utilized here for the proposed HAMR. This HAMR system could potentially exhibit behavior which is more advantageous than either the membrane or the adsorptive reactor, in terms of attaining a nearly complete conversion at the LTS range for improving the hydrogen production efficiency and reducing CO contaminant level. In addition, the HAMR system allows potentially greater process flexibility than either the membrane or the adsorptive reactor system, which could benefit the CO_2 sequestration. For example:

- The HAMR system with the CO_2-adsorbent packed in the reactor and/or permeate sides allows the concentration of CO_2 in the adsorbed phase for disposal during the regenerative phase. Membranes with a strong H_2 affinity will be recommended here.
- The HAMR system with the CO_2-adsorbent packed in the permeate side promotes CO_2 permeation from the reaction side by maintaining the low partial pressure of CO_2 in the permeate side. Membranes with both CO_2 and H_2 affinities will be recommended here.
- The HAMR system with the CO_2-adsorbent packed in the permeate side can deliver a high purity hydrogen as a product stream while removing both WGS reaction products, i.e., CO_2 and H_2, to promote the WGS conversion substantially. Membranes with both CO_2 and H_2 affinities will be recommended here.

The HAMR was originally proposed by our group[1-2, 28], couples the reaction and membrane separation steps with adsorption on the reactor and/or membrane permeate side. The HAMR system investigated previously involved a hybrid pervaporation membrane reactor system, and integrated the reaction and pervaporation step through a membrane with water adsorption. Coupling reaction, pervaporation and adsorption significantly improved the performance. Most recently, Elnashaie and coworkers[7,29-32] mathematically analyzed the behavior of a circulating fluidized-bed HAMR system utilizing Pd membranes. This reactor is assumed to operate at steady-state by recirculating the catalyst and adsorbent through a second reactor for regeneration. The ability of Pd membranes to withstand the rigors of the fluidized-bed steam-reforming environment and of the adsorbents to undergo continuous recirculation and regeneration still remain the key challenges. In addition, this system is not well-suited for on-board or small-scale applications.

In this quarterly report, an improved mathematical model for the HAMR system based upon the previous work (xxxx), primarily with the incorporation of time as an independent variable, is presented for simulating the three opportunities identified above. In the next quarterly report, we will complete the simulation to demonstrate the unique advantages of using the CO_2-affinity adsorbent and membrane developed from this project.

4. RESULTS AND DISCUSSION

4.1. Kinetics for water-gas-shift reaction

For the water gas shift reaction, we utilize a catalytic reaction scheme first proposed by Xu and Froment[8], which has since found wide-spread application for steam reforming reaction. The rate expression, heat of reaction, and the thermodynamic constant for the WGS are shown in Table 1. The kinetic parameters, as reported by Xu and Froment[8], are shown in Table 2. Formation rates for the H_2, CO and CO_2 products and the disappearance rates for H_2O are given by the following equations:

$$R_{H2} = r_2 \quad (1)$$

$$R_{CO} = -r_2 \quad (2)$$

$$R_{CO2} = +r_2 \quad (3)$$

$$R_{H2O} = -r_2 \quad (5)$$

4.2. The mathematical model of the HAMR system

A schematic of the HAMR system is shown in Fig. 1. In this figure the catalyst and adsorbent are packed in the feed side of the membrane (signified by the superscript F, for feed side), with additional adsorbent also packed in the interior of the membrane volume (signified by the superscript P, or permeate side). Of course, there are many options for this proposed reactor, as previously noted. For example, the catalyst may be loaded in the feed side, while the adsorbent may be loaded in the permeate side. Or the catalyst and adsorbent may only be loaded in the feed side, with no adsorbent or catalyst being present in the permeate side. To simplify matters, in the development of the model we assume that the reactor operates isothermally, that external mass transfer resistances are negligible for the transport through the membrane as well as for the catalysts, and that internal diffusion limitations for the catalyst, and internal or external transport limitations for the adsorbent, are accounted for by overall rate coefficients. Moreover, plug-flow conditions are assumed to prevail for both the permeate and feed sides of the membrane, as well as ideal gas law conditions.

In the simulations reported here we utilize the experimentally-measured transport characteristics of a microporous inorganic membrane with the affinity to CO_2. However, due to the presence of the micropores, this membrane also demonstrartes significant affinity to H_2. Through membrane synthesis, the relative contribution between CO_2 and H_2 permeances can be

tailored within a certain range for a particular application. The selectivity between CO_2/H_2 will be part of our simulation study. Mass transfer through the porous membrane is described by the following empirical equation:

$$F_j = U_j(P_j^F - P_j^P) \tag{6}$$

where F_j is the molar flux (mol/m^2.s), P_j^F the partial pressure of component j on the membrane feed side (bar), P_j^P the partial pressure of component j on the membrane permeate side (bar), and U_j the membrane permeance for component j (mol/m^2.bar.s). The membranes are highly permselective towards hydrogen, and CO_2 while rejecting CO effectively.

The mass balance on the feed side of the reactor packed with the WGS catalyst and, potentially, an adsorbent is described by the following equations for CO_2, CO, H_2, H_2O, and an inert species (potentially used as a sweep gas or a blanketing agent:

$$e^F \frac{\partial C_j^F}{\partial t} + \frac{\partial n_j^F}{\partial V} = -a_m U_j(P_j^F - P_j^P) + (1-e_b^F) b_c r_c R_j^F - (1-e_b^F)(1-b_c) r_a G_j^F$$

$$+ e_b^F (A^F)^2 \frac{\partial}{\partial V}\left(D_L^F \frac{\partial C_j^F}{\partial V} \right); \quad \text{j=1,2,…, n} \tag{7}$$

In the above equation n_j^F is the molar flow rate (mol/s) for species j, C_j^F is the gas phase concentration (kmol/m^3) equal to (n_j^F / Q^F), where Q^F is the volumetric flowrate (m^3/s). V is the feed side reactor volume variable (m^3), A^F the cross sectional area for the reactor feed side (m^2), a_m the membrane area per feed side reactor volume (m^2/m^3), e_b^F the bed porosity on the feed side, e^F the total feed side bed porosity (it includes the bed porosity and the catalyst porosity), b_c the fraction of the solid volume occupied by catalysts ($b_c = 1$, when no adsorbent is present), r_c the catalyst and r_a the adsorbent densities (kg/m^3), and R_j^F the reaction rate expression, which is either described by Equations 1-5 above (mol/kg.s), or is equal to zero if j is an inert species. Assuming that the adsorbent only adsorbs CO_2, G_j^F is zero for all other components except CO_2. D_L^F (m^2/s) is the axial dispersion coefficient described by the following equation[34]:

$$D_L^F = 0.73D_m^F + \frac{0.5u^F d_P^F}{1+9.49\frac{D_m^F}{u^F d_P^F}} \quad (8)$$ where D_m^F is molecular diffusivity (m^2/s), u^F is velocity at feed side (m/s), and d_P^F is the particle diameter in feed side (m).

One finds a number of approaches in the literature for describing $G_{CO_2}^F$. Ideally, one would like to account explicitly for both external and internal mass transport, and finite rates of adsorption. Such an approach goes beyond the scope of this preliminary investigation. Traditionally, in the modeling of adsorptive reactors, simpler models have been utilized, instead[22, 27]. Two such models have received the most attention. They are, (i) the model based on the assumption of an instantaneous local adsorption equilibrium (ILE) between the gas and the adsorbent phases [2, 22, 27,28], and (ii) the linear driving force models (LDF), according to which[35] $G_{CO_2}^F$ is described by the following expression:

$$\frac{dC_s}{dt} = G_{CO_2}^F = k_a(C_{s_{eq}} - C_s) \quad (9)$$

where $C_{s_{eq}}$ is the adsorption equilibrium CO_2 concentration on the adsorbent (mol/kg) corresponding to the prevailing gas-phase concentration, C_s is the existing adsorbed CO_2 concentration (mol/kg), and k_a (s^{-1}) is a parameter which "lumps" together the effects of external and intraparticle mass transport and the sorption processes, and which, as a result, is often a strong function of temperature and pressure[27] – though, typically, in modeling it is taken as temperature/pressure independent. Previously we showed that the CO_2 adsorption on this adsorbent follows a Langmuir adsorption isotherm under both dry and wet conditions, described by the following equation.

$$C_{s_{eq}} = \frac{m_{CO_2} b_{CO_2} P_{CO_2}}{1+b_{CO_2} P_{CO_2}} \quad (10)$$

where m_{CO_2} (mol/kg) is the total adsorbent capacity, and b_{CO_2} (bar^{-1}) the adsorption equilibrium constant, which is described by the van't Hoff equation

$$b_{CO_2} = b_{CO_2}(T_0)\exp(-\Delta H_a / R(1/T - 1/T_0)) \quad (11)$$

The heat of adsorption ΔH_a (kJ/mol) under wet conditions for a region of temperatures from 481 -753 K was calculated to be -17 kJ/mol, while b_{CO_2} at 673 K is equal to 23.6 bar [27].

Equations 7 and 9 must be complemented by initial and boundary conditions. For simplicity, we assume here that the reactor, prior to the initiation of the reaction/adsorption step, has undergone a start-up procedure as described by Ding and Alpay[22], which involves, (i) heating up the reactor to the desired temperature under atmospheric pressures by feeding H_2 in the reactor feed side and the chosen sweep gas on the permeate side; (ii) supplying water to the system so that the feed H_2O:H_2 ratio is the same with the H_2O:CO ratio to be used during the reaction step; (iii) pressurizing the feed and permeate side to the desired pressure conditions, and (iv) switching from H_2 to CO to initiate the reaction/adsorption step. In the simulations the conditions prevailing at the start of step of step (iv) are those prevailing at steady state during step (iii). In addition, during step (iv) the following conventional boundary conditions prevail [16-20]:

$$@V = 0; \qquad \frac{\partial x_j^F}{\partial V} = -\frac{u_0^F (x_{j0}^F - x_j^F)}{A^F e_b^F D_L^F} \tag{12a}$$

$$@V = V_R; \qquad \frac{\partial x_j^F}{\partial V} = 0 \tag{12b}$$

where u_0^F is the inlet superficial velocity (m/s), V_R the total reactor volume (m^3), x_j^F the mole fraction and x_{j0}^F the inlet mole fraction for species j.

Assuming that the catalyst and adsorbent particles have the same size, the pressure drop in a packed bed can be calculated using the Ergun equation:

$$-\frac{dP^F}{dV} = 10^{-6}\,\frac{f^F \left(G_m^F\right)^2}{A^F g_c d_P^F r_F^F} \tag{13}$$

$$\text{at V=0, } P^F = P_0^F \tag{13a}$$

$$f^F = \left(\frac{1-e_b^F}{\left(e_b^F\right)^3}\right)\left(1.75 + \frac{150\left(1-e_b^F\right)}{N_{\mathrm{Re}}^F}\right) \tag{13b}$$

$$N_{\mathrm{Re}}^F < 500\left(1-e_b^F\right) \tag{13c}$$

$$N_{\mathrm{Re}}^F = \frac{d_P^F G_m^F}{m^F} \tag{13d}$$

where, P^F is the feed side pressure (bar), P_0^F the inlet feed side pressure, m^F the viscosity (Pa.s), d_P^F the particle diameter in feed side (m), $G_m^F = r_F^F u^F$ the superficial mass flow velocity in the feed side (kg/m^2.s), r_F^F the density of the fluid (kg/m^3), and g_c the gravity conversion factor equal to one in SI units.

During the initial simulation, we assume that no adsorbent or catalyst is present in the permeate side. For the permeate side, the following equation is, therefore, utilized:

$$\frac{\partial C_j^P}{\partial t} + k\frac{\partial n_j^P}{\partial V} = a_m k U_j (P_j^F - P_j^P) + \left(A^F\right)^2 \frac{\partial}{\partial V}\left(D_L^P \frac{\partial C_j^P}{\partial V}\right) \qquad \text{j=1,2,…,n} \qquad (14)$$

where $k = \frac{A^F}{A^P}$, A^P being the cross-sectional area on the permeate side (m^2), and D_L^P (m^2/s) is the axial Taylor-Aris dispersion coefficient on the permeate side[36] given as

$$D_L^P = D_m^P + \frac{\left(u^P\right)^2 \left(d_t^P\right)^2}{192 D_m^P} \qquad (15)$$

where D_m^P is the molecular diffusivity (m^2/s), u^P is the velocity at the permeate side (m/s) and d_t^P is membrane inside diameter (m). In the simulations, the conditions prevailing in the permeate side at the start of step (iv) are those prevailing at steady state during step (iii). In addition, during step (iv) the following conditions prevail in the permeate side,

$$@V = 0; \qquad \frac{\partial x_j^P}{\partial V} = -\frac{u_0^P (x_{j0}^P - x_j^P)}{A^F D_L^P} \qquad (16a)$$

$$@V = V_R; \qquad \frac{\partial x_j^P}{\partial V} = 0 \qquad (16b)$$

where x_j^P is the mole fraction, x_{j0}^P the inlet mole fraction for species j on the permeate side and u_0^P the superficial flow velocity (m/s) at the inlet. Since no adsorbent or catalyst is present in the permeate side, we ignore any potential pressure drops.

The reactor conversion (based on methane, which is typically the limiting reagent) is defined by the following equation:

$$X_{CO} = \frac{n_{CO}^F - \left(n_{CO}^F + n_{CO}^P\right)}{n_{CO}^F} \qquad (17)$$

where n_{CO}^F is the inlet molar flow rate of CO, and $n_{CO,ex}^F$, and $n_{CO,ex}^P$ are the CO molar flow rates at the exit of the reactor feed and permeate sides correspondingly (mol/s). The yield of product hydrogen is defined by the following equation:

$$Y_{H_2} = \frac{1}{4} \times \frac{(n_{H_2,ex}^F - n_{H_{20}}^F) + (n_{H_2,ex}^P - n_{H_{20}}^P)}{n_{CO0}^F} \qquad (18)$$

where $n^F_{H_2,ex}$ and $n^P_{H_2,ex}$ are, respectively the hydrogen molar flow rates at the exit of the reactor feed and permeate sides, and $n^F_{H_20}$ and $n^P_{H_20}$ the H_2 molar flow rates potentially present at the inlet of the reactor feed and permeate sides (mol/s).

Equations 6-18 can be written in dimensionless form by defining the following variables and groups:

$$t_a = (k_a)^{-1}; t_F = \frac{e^F V_R}{A^F u_0^F}; g = \frac{t_F}{t_a}; h = \frac{V}{V_R}; u^F = \frac{Q^F}{A^F}; u_0^F = \frac{Q_0^F}{A^F}; x^F = \frac{u^F}{u_0^F}; x^P = \frac{u^P}{u_0^P};$$

$$\Psi^F = \frac{P^F}{P_0^F}; \Psi^P = \frac{P^P}{P_0^P}; w = \frac{P_0^P}{P_0^F}; a_j = \frac{MW_j}{MW_{H_2}}; x_j^F = \frac{P_j^F}{P^F}; x_j^P = \frac{P_j^P}{P^P}; t = k_a t; d_j = \frac{U_j}{U_{H_2}};$$

$$K'_{eq1} = \frac{K_{eq1}}{(P_0^F)^2}; \quad K'_{CO} = K_{CO} P_0^F; \; K'_{H_2} = K_{H_2} P_0^F; \; b_{CO_2} = b_{CO_2} P_0^F$$

$$Da = \frac{b_c (1 - e_b^F) r_c k_1(T_0) V_R RT}{A^F u_0^F (P_0^F)^{1.5}}; \; Pe = \frac{A^F u_0^F}{U_{H_2} V_R a_m RT}; \Theta^F = \frac{e_b^F A^F D_L^F}{u_0^F V_R}; \Theta^P = \frac{A^F D_L^P}{u_0^P V_R}$$

$$Ha = \frac{(1 - b_c)(1 - e_b^F) V_R r_a k_a RT m_{CO_2}}{A^F u_0^F P_0^F}; \; \Lambda = \frac{Ha}{Da}; \; \Omega = (Da)(Pe);$$

$$\Xi = 10^{-6} f^F \frac{(u_0^F)^2 MW_{H_2} V_R}{A^F g_c d_p^F RT}; \; l = \frac{A^P u_0^P}{A^F u_0^F}; \; q^F_{seq} = \frac{C^F_{seq}}{m_{CO_2}}; \; q^F_s = \frac{C^F_s}{m_{CO_2}};$$

The dimensionless equations equivalent to Eqs. (7 -18) are

$$g \frac{\partial x_j^F}{\partial t} = -\left(x^F \frac{\partial x_j^F}{\partial h} + x_j^F \frac{\partial x^F}{\partial h} + \frac{x_j^F x^F}{\Psi^F} \frac{\partial \Psi^F}{\partial h} \right) - \frac{Da d_j}{\Omega} \left(x_j^F - x_j^P w \frac{\Psi^P}{\Psi^F} \right) + Da \frac{1}{\Psi^F} R'^F_j - Da\Lambda \frac{1}{\Psi^F} G'^F_j +$$

$$+ \Theta^F \frac{\partial^2 x_j^F}{\partial h^2} + 2\Theta^F \frac{1}{\Psi^F} \left(\frac{\partial x_j^F}{\partial h} \right) \left(\frac{\partial \Psi^F}{\partial h} \right); \qquad \text{j=1,2,…, n-1} \qquad (19)$$

$$\frac{\partial x^F}{\partial h} = -\frac{x^F}{\Psi^F} \frac{\partial \Psi^F}{\partial h} - \frac{Da}{\Omega} \sum_j d_j \left(x_j^F - x_j^P w \frac{\Psi^P}{\Psi^F} \right) + Da \frac{1}{\Psi^F} \sum_j R'^F_j - \Lambda Da \frac{1}{\Psi^F} G'^F_{CO_2} \qquad (20)$$

$$\frac{g}{e^F l k} \frac{\partial x_j^P}{\partial t} = -\left(x^P \frac{\partial x_j^P}{\partial h} + x_j^P \frac{\partial x^P}{\partial h} + \frac{x_j^P x^P}{\Psi^P} \frac{\partial \Psi^P}{\partial h} \right) + \frac{Da\, d_j}{l\, \Omega} \left(x_j^F \frac{\Psi^F}{w \Psi^P} - x_j^P \right) +$$

$$\Theta^P \frac{\partial^2 x_j^P}{\partial h^2} + 2\Theta^P \frac{1}{\Psi^P}\left(\frac{\partial x_j^P}{\partial h}\right)\left(\frac{\partial \Psi^P}{\partial h}\right); \quad \text{j=1,2,..., n-1} \tag{21}$$

$$\frac{\partial x^P}{\partial h} = -\frac{x^P}{\Psi^P}\frac{\partial \Psi^P}{\partial h} + \frac{Da}{l\Omega}\sum_j d_j\left(x_j^F \frac{\Psi^F}{w\Psi^P} - x_j^P\right) \tag{22}$$

$$\frac{\partial \Psi^F}{\partial h} = -\Xi(x^F)^2 \Psi^F \sum x_j^F a_j \tag{23}$$

$$\frac{dq_S^F}{dt} = q_{S_{eq}}^F - q_S^F \tag{24}$$

$$X_{CO} = \frac{x_{CH_{4_0}}^F - \left(x_{CO}^F \Psi^F x^F\right)_{ex} + \left(x_{CO}^P l \Psi^P w x^P\right)_{ex}}{x_{CO_0}^F} \tag{25}$$

$$Y_{H_2} = \frac{1}{4} \times \frac{(x_{H_2}^F \Psi^F x^F)_{ex} - x_{H_{2_0}}^F + (x_{H_2}^P l \Psi^P w x^P)_{ex} - x_{H_{2_0}}^P l w}{x_{CO_0}^F} \tag{26}$$

where, in dimensionless form

$$G'^F_{CO_2} = (q_{seq}^F - q_s^F) \tag{27}$$

$$q_{seq}^F = \frac{b_{CO_2} x_{CO_2}^F \Psi^F}{1 + b_{CO_2} x_{CO_2}^F \Psi^F} \tag{28}$$

and R'_j are dimensionless forms of R_i that are described by Eqs. (1-5) above with the dimensionless form of the rates $r'_1 - r'_3$ shown in Table 3. Equations (20) and (22) that express the dimensionless velocity distributions are obtained by overall mass balances on the in the feed and permeate side. In the absence of substantial pressure drop in the permeate side in Eq. (21), $\Psi^P = 1$, and $\frac{\partial \Psi^P}{\partial h} = 0$. The initial conditions at the start of the adsorption/reaction step are those prevailing during step 3 previously described. In addition, the following boundary conditions also apply:

$$t > 0;\ @h = 0; \quad ?^F = 1\ ;\ ?^P = 1 \tag{29a}$$

$$x^F = 1\ ;\ x^P = 1 \tag{29b}$$

$$\frac{\partial x_j^F}{\partial h} = -\frac{1}{\Theta^F}(x_{j0}^F - x_j^F);\ i = 1, 2, ..., n \tag{29c}$$

$$\frac{\partial x_j^P}{\partial h} = -\frac{1}{\Theta^P}(x_{j0}^P - x_j^P);\ i = 1, 2, ..., n \tag{29d}$$

$$t > 0; @\, h = 1; \; \frac{\partial x_j^F}{\partial h} = 0 \tag{30a}$$

$$\frac{\partial x_j^P}{\partial h} = 0 \tag{30b}$$

where, $s = \dfrac{\sum n_{j0}^P}{\sum n_{j0}^F} = l\,w \dfrac{\sum x_{j0}^P}{\sum x_{j0}^F}$ is the sweep ratio for the membrane reactor.

The system of coupled non-linear partial differential Equations (19-24) and accompanying boundary conditions has been solved in MATLAB using the method of lines (MOL)[37, 38]. The system of partial differential equations were converted to a set of ordinary differential equations by discretizing the spatial derivative in h direction using a five-point biased upwind finite differences scheme to approximate the convective term. A fourth-order central differences scheme has been used to approximate the diffusive term. For finite differences, the reactor volume was divided into n sections with (n+1) nodes. The initial value ordinary differential equations and other explicit algebraic equations at a time t were simultaneously solved using 'ode45.m', a MATLAB built-in solver for initial value problems for ordinary differential equations.

5. CONCLUSIONS

The HAMR system we proposed can potentially take the full advantage of the CO_2-based adsorbent and membrane developed from this project for improving hydrogen production efficiency with concomitant CO_2 removal for sequestration purpose. A complete mathematical model has been developed to describe the HAMR system, which offers process flexibility to incorporate both catalysts and adsorbents in the reactor as well as permeate sides. In comparison with the preliminary mathematical model we have developed previously, this improved model incorporate time as an independent variable to realistically simulate the unsteady state nature of the adsorptive process. In the next quarterly report, we will complete the simulation to demonstrate the potential benefit of the proposed process based upon the performance parameters obtained from the CO_2-affinity adsorbent and membrane developed from this project.

Bibliography:

(1) Park B. *Models and Experiments with Pervaporation Membrane Reactors Integrated with a Water Removal Adsorbent System*, Ph.D. Thesis, University of Southern California, Los Angeles, California, 2001.

(2) Park, B.; Tsotsis, T. T. Models and Experiments with Pervaporation Membrane Reactors Integrated With an Adsorbent System. *Chem. Eng. Proc*. **2004**, 43, 1171.

(3) Choi, Y.; Stenger, H.G. Water Gas Shift Reaction Kinetics and Reactor Modeling for Fuel Cell Grade Hydrogen. J. Power Sources **2003,** 124, 432.

(4) Darwish, N. A.; Hilal, N.; Versteeg, G.; Heesink, B. Feasibility of the Direct Generation of Hydrogen for Fuel-cell-powered Vehicles by on-board Steam Reforming of Naphtha. *Fuel.* **2003**, 83, 409.

(5) Liu, Z.; Roh, H.; Park, S. Hydrogen Production for Fuel Cells Through Methane Reforming at Low Temperatures. J. Power Sources **2002,** 111, 83.

(6) Semelsberger, T. A.; Brown, L. F.; Borup, R. L.; Inbody, M. A. Equilibrium Products from Autothermal Processes for Generating Hydrogen-rich Fuel-cell Feeds. *Int. J. Hydrogen Energ.* **2004**, 29, 1047.

(7) Elnashaie, S.S.E.H.; Adris, A.; Al-Ubaid, A.S.; Soliman, M.A. On the Non-monotonic Behavior of Methane-steam Reforming Kinetics. *Chem. Eng. Sci.* **1990,** 45, 491.

(8) Xu, J.; Froment, G.F. Methane Steam Reforming, Methanation and Water-gas Shift: I. Intrinsic Kinetics. *AIChE J*. **1989,** 35, 88.

(9) Han, C.; Harrison, D.P. Simultaneous Shift Reaction and Carbon Dioxide Separation for the Direct Production of Hydrogen. *Chem. Eng. Sci.* **1994,** 49, 5875.

(10) Hwang, S. Inorganic Membranes and Membrane Reactors, *Korean J. Chem. Eng.* **2001,** 18, 775.

(11) Lim, S.Y.; Park, B.; Hung, F.; Sahimi, M.; Tsotsis, T.T. Design Issues of Pervaporation Membrane Reactors for Esterification. *Chem. Eng. Sci.* **2002,** 57, 4933.

(12) Park, B.; Ravi-Kumar, V.S.; Tsotsis, T.T. Models and Simulation of Liquid-phase Membrane Reactors. *Ind. Eng. Chem. Res*. **1998,** 37, 1276.

(13) Nam, S.W.; Yoon, S.P.; Ha, H.Y.; Hong, S.; Maganyuk, A.P. Methane Steam Reforming in a Pd-Ru Membrane Reactor. *Korean J. Chem. Eng.* **2000,** 17, 288.

(14) Saracco, G.; Specchia, V. Catalytic Inorganic-membrane Reactors: Present Experience and

Future Opportunities. *Catal. Rev.-Sci. Eng*. **1994,** 36, 305.

(15) Sanchez, J.; Tsotsis, T.T. *Catalytic Membranes and Membrane Reactors*; Wiley-VCH: Weinheim, 2002.

(16) Xiu, G. H.; Li, P.; Rodrigues, A. E. Subsection-controlling Strategy for Improving Sorption-enhanced Reaction Process. *Chem. Eng. Res. Des*. **2004**, 82, 192.

(17) Xiu, G.; Li, P.; Rodrigues, A. E. Adsorption-enhanced Steam-methane Reforming with Intraparticle-diffusion Limitations**.** *Chem. Eng. J*. (Amsterdam, Netherlands) **2003**, 95, 83.

(18) Xiu, G.; Li, P.; Rodrigues, A. E. New Generalized Strategy for Improving Sorption-enhanced Reaction Process. *Chem. Eng. Sci*. **2003**, 58, 3425.

(19) Xiu, G.; Soares, J. L.; Li, P.; Rodrigues, A. E. Simulation of Five-step One-bed Sorption-enhanced Reaction Process. *AIChE J*. **2002**, 48, 817.

(20) Xiu, G.; Li, P.; Rodrigues, A. E. Sorption-enhanced Reaction Process with Reactive Regeneration. *Chem. Eng. Sci*. **2002**, 57, 3893.

(21) Lee, D. K.; Baek, I. H.; Yoon, W. L. Modeling and Simulation for the Methane Steam Reforming Enhanced by in Situ CO_2 Removal Utilizing the CaO Carbonation for H_2 Production. *Chem. Eng. Sci*. **2004**, 59, 931.

(22) Ding, Y.; Alpay, E. Adsorption-enhanced Steam-methane Reforming. *Chem. Eng. Sci*. **2000**, 55, 3929.

(23) Ortiz, A. L.; Harrison, D. P. Hydrogen Production Using Sorption-Enhanced Reaction. *Ind. Eng. Chem. Res*. **2001**, 40, 5102.

(24) Balasubramanian, B.; Ortiz, A. L.; Kaytakoglu, S.; Harrison, D. P. Hydrogen from Methane in a Single-step Process. *Chem. Eng. Sci*. **1999**, 54, 3543.

(25) Waldron, W. E.; Hufton, J. R.; Sircar, S. Production of Hydrogen by Cyclic Sorption Enhanced Reaction Process. *AIChE J*. **2001**, 47, 1477.

(26) Hufton, J. R.; Mayorga, S.; Sircar, S. Sorption-enhanced Reaction Process for Hydrogen Production. *AIChE J*. **1999**, 45, 248.

(27) Ding, Y.; Alpay, E. Equilibria and Kinetics of CO_2 Adsorption on Hydrotalcite Adsorbent. *Chem. Eng. Sci*. **2000**, 55, 3461.

(28) Park, B. A Hybrid Adsorbent-membrane Reactor (HAMR) System for Hydrogen Production. *Korean J. Chem. Eng*. **2004**, 21, 782.

(29) Chen, Z.; Elnashaie, S. S. E. H. Bifurcation Behavior and Efficient Pure Hydrogen Production for Fuel Cells Using a Novel Autothermic Membrane Circulating Fluidized-Bed (CFB) Reformer:

Sequential Debottlenecking and the Contribution of John Grace. *Ind. Eng. Chem. Res.* **2004**, 43, 5449.

(30) Prasad, P.; Elnashaie, S. S. E. H. Novel Circulating Fluidized-Bed Membrane Reformer Using Carbon Dioxide Sequestration. *Ind. Eng. Chem. Res.* **2004**, 43, 494.

(31) Prasad, P.; Elnashaie, S. S. E. H. Coupled Steam and Oxidative Reforming for Hydrogen Production in a Novel Membrane Circulating Fluidized-Bed Reformer. *Ind. Eng. Chem. Res.* **2003**, 42, 4715.

(32) Chen, Z.; Yan, Y.; Elnashaie, S. S. E. H. Novel Circulating Fast Fluidized-bed Membrane Reformer for Efficient Production of Hydrogen from Steam Reforming of Methane. *Chem. Eng. Sci.* **2003**, 58, 4335.

(33) Ciora, R. J.; Fayyaz, B.; Liu, P. K. T.; Suwanmethanond, V.; Mallada, R.; Sahimi, M.; Tsotsis, T. T. Preparation and Reactive Applications of Nanoporous Silicon Carbide Membranes. *Chem. Eng. Sci.* **2004**, 59, 4957.

(34) Edwards, M. F.; Richardson, J. F. Gas Dispersion in Packed Beds. *Chem. Eng. Sci.* **1968**, 23, 109.

(35) Karger, J.; Ruthven, D.M. *Diffusion in Zeolites and Other Microporous Solids*; Wiley Publishers: New York, 1992.

(36) Levenspiel, O. *Chemical Reaction Engineering*, 3rd Edition**;** Wiley: New York, 1998**.**.

(37) Schiesser, W. E. *The Numerical Method of Lines: Integration of Partial Differential Equations*; Academic Press: San Diego, 1991.

(38) Vande Wouwer, A.; Saucez, P.; Schiesser, W. E. Simulation of Distributed Parameter Systems Using a Matlab-Based Method of Lines Toolbox: Chemical Engineering Applications. *Ind. Eng. Chem. Res.* **2004**, 43, 3469.

Vasileiadis, S. P. *Catalytic Ceramic Membrane Reactors for the Methane-Steam Reforming Reaction: Experiments and Simulation*, Ph.D. Thesis, University of Southern California, Los Angeles, California 1994

Acronyoms :

A^F	cross sectional area for the reactor feed side (m^2)
A^P	cross sectional area for the reactor permeate side (m^2)
b_{CO_2}	Langmuir model adsorption equilibrium constant for CO_2 (bar^{-1})
C_j^F	gas phase concentration of species j in the feed side ($kmol/m^3$)
C_j^P	gas phase concentration of species j in the permeate side ($kmol/m^3$)
C_s	solid phase concentration of CO_2 (mol/kg)
C_{seq}	equilibrium solid phase concentration of CO_2 (mol/kg)
Da	Damkohler number (dimensionless)
D_L^F	axial dispersion coefficient in the feed side (m^2/s)
D_L^P	axial dispersion coefficient in the permeate side (m^2/s)
D_m^F	molecular diffusivity in feed side(m^2/s)
D_m^P	molecular diffusivity in permeate side (m^2/s)
d_t^p	membrane inside diameter (m)
d_p^F	particle diameter in feed side (m)
f^F	friction factor (dimensionless)
F_j	molar flux ($mol/m^2.s$)
g_c	gravity conversion factor
G_m^F	superficial mass flow velocity in the feed side ($kg/m^2.s$)
$G_j^{'F}$	dimensionless adsorption rate for species j
G_j^F	adsorption rate for species j (mol/kg.s)
Ha	Hatta number (dimensionless)
k	A^F/A^P
k_a	LDF mass transfer coefficient (s^{-1})
K_{H2O}	dissociative adsorption constant of water
K'_{CO}	dimensionless kinetic parameter (dimensionless)
K_{eq2}	equilibrium constant of reaction II in Table 1. (dimensionless)
m_{CO2}	Langmuir model total adsorbent capacity constant for CO_2 (mol/kg)
MW_j	molecular weight of species j

N^{F}_{Re}	Reynolds number for feed side
$n^{F}_{j_0}$	inlet molar flow rate for feed side (mol/s)
$n^{P}_{j_0}$	inlet molar flow rate for permeate side (mol/s)
n_j^F	molar flow rate for component *j* in the feed side (mol/s)
n_j^P	molar flow rate for component *j* in the permeate side (mol/s)
$n^{F}_{i,ex}$	molar flow rates at the exit of the reactor for component *i* in the feed side (mol/s)
$n^{P}_{i,ex}$	molar flow rates at the exit of the reactor for component *i* in the permeate side (mol/s)
P_0^F	inlet feed side pressure(bar)
Pe	Peclet Number
P^F	feed side pressure (bar)
P_j^F	partial pressure of component j in the membrane feed side (bar)
P_j^P	partial pressure of component j in the membrane permeate side (bar)
Q_0^F	volumetric flow rate (m^3/s)
R	ideal gas constant (m^3.bar/mol.K)
r_i	rate of reaction for i^{th} equation (kmol/kg.s)
r_i'	dimensionless rate of reaction for i^{th} equation
R_j	reaction rate expression for species j (kmol/kg.s)
R'_j	dimensionless reaction rate expression for species j
s	sweep ratio
t	time (second)
T	absolute temperature (K)
T_0	reference temperature (K)
u_0^F	superficial flow velocity at the inlet on feed side (m/s)
u_0^P	superficial flow velocity at the inlet on permeate side (m/s)
u^F	superficial flow velocity on feed side (m/s)
u^P	superficial flow velocity on permeate side (m/s)
U_j	membrane permeance for component *j* (mol/m^2.bar.s)
V	reactor volume (m^3)
V_R	total reactor volume (m^3)

W_c	catalyst weight (kg)
X_{CH_4}	methane conversion (dimensionless)
$x_{j_0}^F$	inlet mole fraction for species j in the feed side
$x_{j_0}^P$	inlet mole fraction for species j in the permeate side
x_j^F	mole fraction for species j in the feed side
x_j^P	mole fraction for species j in the permeate side
y_j	mole fraction of component j
Y_{H_2}	hydrogen yield (dimensionless)

Subscripts

0	entrance condition
ads	adsorbent condition
eq.	equilibrium
ex	exit
j	chemical species

Superscripts

F	feed side
P	permeate side

Greek Letters

a_m	membrane area per feed side reactor volume (m^2/m^3)
a_j	MW_j/MW_{H2}
b_c	fraction of the reactor volume occupied by catalysts
b_{CO_2}	$b_{CO_2} P_0^F$ (dimensionless)
g	t_F / t_a (dimensionless)

ΔH_a	heat of adsorption (kJ/mol)
d_j	separation factor (dimensionless)
e^F	total feed side bed porosity
e_b^F	bed porosity in the feed side
x^F	u^F / u_0^F (dimensionless)
x^P	u^P / u_0^P (dimensionless)
h	V/V_R (dimensionless)
Θ^F	$e_b^F A^F D_L^F / u_0^F V_R$ (dimensionless)
Θ^P	$A^F D_L^P / u_0^P V_R$ (dimensionless)
q_s^F	C_s^F / m_{CO_2} ,(dimensionless)
q_{seq}^F	C_{seq}^F / m_{CO_2} ,(dimensionless)
Λ	Ha/Da (dimensionless)
l	$A^P u_0^P / A^F u_0^F$ (dimensionless)
m^F	viscosity (Pa.s)
Ξ	$10^{-6} f^F ((u_0^F)^2 MW_{H_2} V_R / A^F g_c d_p^F RT)$ (dimensionless)
r_a	adsorbent density (kg/m^3)
r_c	catalyst density (kg/m^3)
r_F^F	fluid density (kg/m^3)
t	$k_a t$ (dimensionless)
t_F	$e^F V_R / A^F u_0^F$ (dimensionless)
t_a	$(k_a)^{-1}$ (dimensionless)
Ψ^F	P^F / P_0^F (dimensionless)
Ψ^P	P^P / P_0^P (dimensionless)
Ω	(Da)(Pe) (dimensionless)

w	P_0^P / P_0^F	(dimensionless)

Table 1
Rate expressions and thermodynamic properties for the water gas shift reaction

i	reactions	rate expressions	heat of reaction at 298K ΔH_R^0 (kJ/mol)	equilibrium constant, K_{eqi}
1	$CO + H_2O \Leftrightarrow CO_2 + H_2$	$r_2 = \dfrac{\dfrac{k_2}{P_{H_2}}\left(P_{CO}P_{H_2O} - \dfrac{P_{H_2}P_{CO_2}}{K_{eq2}}\right)}{(DEN)^2}$	-41.15	$K_{eq2} = \exp\left[-4.036 + \dfrac{4{,}400}{T}\right]$

$$DEN = 1 + K_{CO}P_{CO} + K_{H_2}P_{H_2} + K_{CH_4}P_{CH_4} + K_{H_2O} \cdot P_{H_2O} / P_{H_2}$$

Table 2
Kinetic parameters for the water gas shift reaction[8]

kinetic parameters	pre-exponential terms, k_{i0}, K_{i0}	activation energies or heats of chemisorption, E_a, DH, kJ/mol	units
k_2	1.955×10^{6}	67.13	kmol/kg-cat/hr/bar
K_{CO}	8.23×10^{-5}	-70.65	bar^{-1}
K_{H_2}	6.12×10^{-9}	-82.90	bar^{-1}
K_{H_2O}	1.77×10^{5}	88.68	-

Table 3
Dimensionless rate expressions for the water gas shift reaction

i	reactions	rate expressions
1	$CO + H_2O \Leftrightarrow CO_2 + H_2$	$r'_2 = \frac{k_2}{k_1} \frac{\left(P_0^F\right)^{1.5} \Psi}{\left(DEN\right)^2 x_{H_2}} \left[x_{CO} . x_{H_2O} - \frac{x_{H_2} x_{CO\,2}}{K_{eq2}} \right]$

$$DEN = 1 + K_{H_2} P_{H_2} + K_{H_2O} \frac{P_{H_2O}}{P_{H_2}}$$

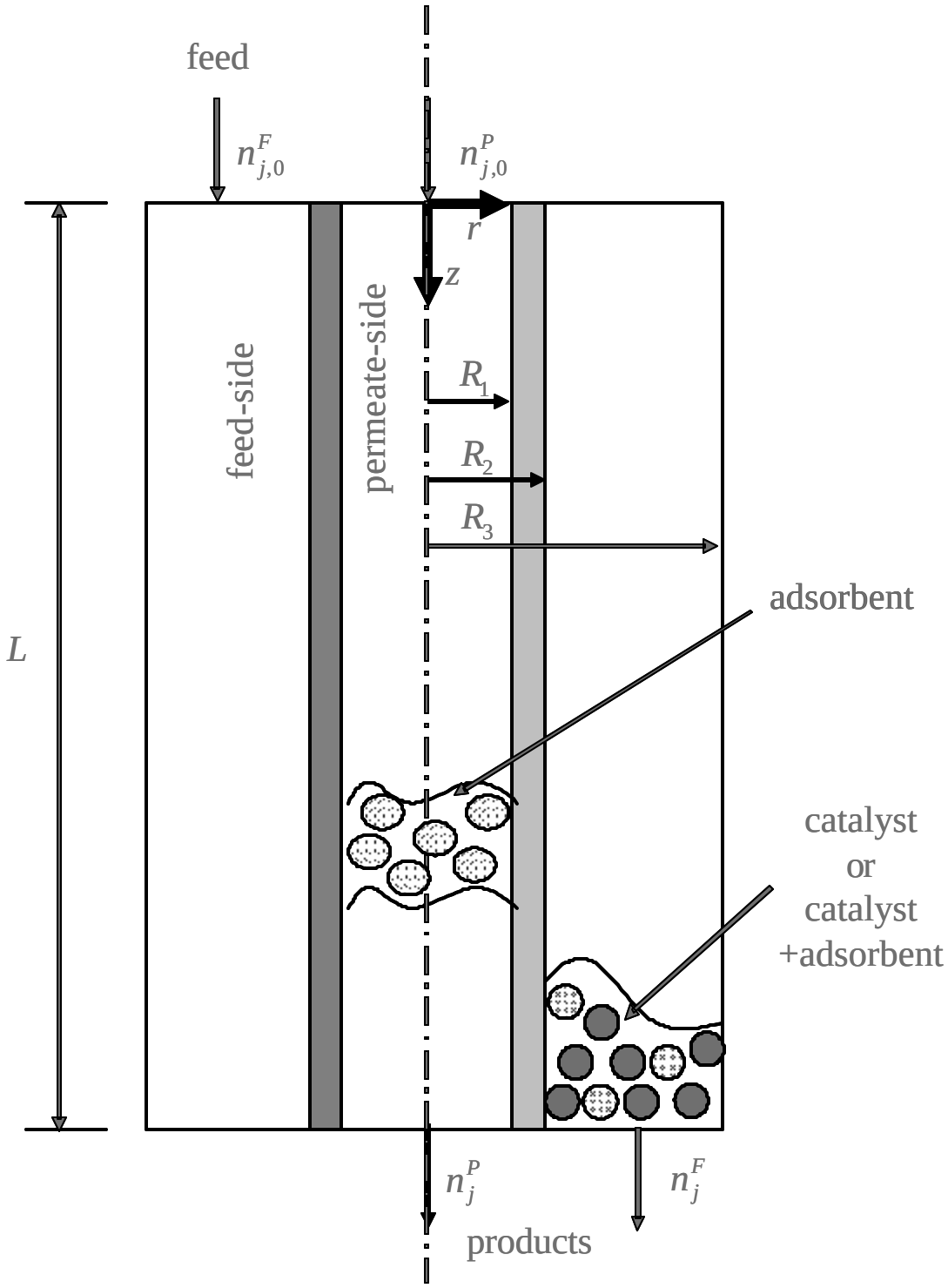

Figure 1. Schematic diagram of a HAMR system.